

<sup>1</sup> MotilA – A Python pipeline for the analysis of  
<sup>2</sup> microglial fine process motility in 3D time-lapse  
<sup>3</sup> multiphoton microscopy data

<sup>4</sup> Fabrizio Musacchio  <sup>1</sup>¶, Sophie Crux<sup>1</sup>, Felix Nebeling<sup>1</sup>, Nala Gockel<sup>1</sup>, Falko  
<sup>5</sup> Fuhrmann<sup>1</sup>, and Martin Fuhrmann  <sup>1</sup>

<sup>6</sup> 1 German Center for Neurodegenerative Diseases (DZNE), Bonn, Germany ¶ Corresponding author

DOI: [10.xxxxxx/draft](https://doi.org/10.xxxxxx/draft)

Software

- [Review](#) ↗
- [Repository](#) ↗
- [Archive](#) ↗

Editor: [Open Journals](#) ↗

Reviewers:

- [@openjournals](#)

Submitted: 01 January 1970

Published: unpublished

License

Authors of papers retain copyright  
and release the work under a  
Creative Commons Attribution 4.0  
International License ([CC BY 4.0](#)).<sup>17</sup>

<sup>7</sup> **Summary**

<sup>8</sup> *MotilA* is an open-source Python pipeline for quantifying microglial fine-process motility in  
<sup>9</sup> 3D time-lapse two-channel fluorescence microscopy. It was developed for high-resolution  
<sup>10</sup> *in vivo* multiphoton imaging and supports single-stack and batch analyses. The workflow  
<sup>11</sup> performs sub-volume extraction, optional registration/unmixing, z-projection, segmentation,  
<sup>12</sup> and pixel-wise change detection to compute the turnover rate (TOR). The code is platform  
<sup>13</sup> independent, documented with tutorials and example datasets, and released under GPL-3.0.

<sup>14</sup> **Statement of need**

<sup>15</sup> Microglia are immune cells of the central nervous system and continuously remodel processes  
<sup>16</sup> to survey brain tissue and respond to pathology ([M. Fuhrmann et al., 2010; Nimmerjahn et al., 2005; Prinz et al., 2019; Tremblay et al., 2010](#)). Quantifying this subcellular motility is  
<sup>17</sup> important for studies of neuroinflammation, neurodegeneration, and synaptic plasticity. Current  
<sup>18</sup> practice in many labs relies on manual or semi-manual measurements in general-purpose tools  
<sup>19</sup> such as Fiji/ImageJ or proprietary software ([Carl Zeiss Microscopy GmbH, Accessed 2025; Schindelin et al., 2012](#)). These procedures are time consuming, hard to reproduce, focus  
<sup>20</sup> on single cells, and are sensitive to user bias ([Brown, 2017; Wall et al., 2018](#)). There is no  
<sup>21</sup> dedicated, open, and batch-capable solution tailored to this task.  
<sup>22</sup>

<sup>23</sup> *MotilA* fills this gap with an end-to-end, reproducible pipeline for 3D time-lapse two-channel  
<sup>24</sup> imaging. It standardizes preprocessing, segmentation, and motility quantification and scales  
<sup>25</sup> from individual stacks to large experimental cohorts. Unlike Fiji/ImageJ macros or proprietary  
<sup>26</sup> packages, *MotilA* provides a fully automated non-interactive workflow in Python that applies  
<sup>27</sup> identical parameters across datasets, logs all intermediate steps, and avoids user-dependent  
<sup>28</sup> adjustments. This ensures reproducible, bias-minimized, and scalable processing of large 3D  
<sup>29</sup> time-lapse datasets, including optional motion correction and spectral unmixing. Although  
<sup>30</sup> optimized for microglia, the approach generalizes to other motile structures that can be reliably  
<sup>31</sup> segmented across time.  
<sup>32</sup>

<sup>33</sup> To clarify *MotilA*'s novelty relative to existing analysis approaches, the following table summarizes  
<sup>34</sup> key differences between *MotilA*, Fiji/ImageJ, and ZEISS ZEN:

<sup>35</sup> **Table 1.** Comparison of MotilA with commonly used alternatives for microglial motility analysis.

Feature	Fiji/ImageJ	ZEISS ZEN	MotilA
<b>Automation</b>	Limited. User-recorded macros; complex workflows often require manual steps and must be split across several macros.	None. Full user interaction required.	Full. End-to-end non-interactive workflow.
<b>Batch processing</b>	Limited. Macros can process several files in one folder, but they cannot navigate nested directory structures or manage multi-step 3D multi-channel time-series pipelines.	None. Each dataset processed manually.	Full. Metadata-driven cohort processing.
<b>Reproducibility</b>	Moderate. Requires complete manual logging; interactive tuning reduces reproducibility.	Low. Manual adjustments introduce strong user bias.	High. Full parameter logging and deterministic runs.
<b>Scalability</b>	Low. Full-stack RAM loading; no chunked I/O for large 3D data.	Low-medium. Efficient viewing but no automated processing for large time-lapse datasets.	High. Chunked I/O for multi-gigabyte 3D two-channel stacks.
<b>Open-source</b>	Yes (GPL-3.0).	No (proprietary).	Yes (GPL-3.0).

### <sup>36</sup> Implementation and core method

<sup>37</sup> Input is a 5D stack in TZCYX or TZYX order, where T is time, Z is depth, C is channel,  
<sup>38</sup> and YX are spatial dimensions. For each time point, *MotilA* extracts a user-defined z-sub-  
<sup>39</sup> volume, optionally performs 3D motion correction and spectral unmixing, and computes a 2D  
<sup>40</sup> maximum-intensity projection to enable interpretable segmentation. After thresholding, the  
<sup>41</sup> binarized projection  $B(t_i)$  is compared with  $B(t_{i+1})$  to derive a change map

$$\Delta B(t_i) = 2B(t_i) - B(t_{i+1}).$$

<sup>42</sup> Pixels are classified as stable “S” ( $\Delta B = 1$ ), gained “G” ( $\Delta B = -1$ ), or lost “L” ( $\Delta B = 2$ ).  
<sup>43</sup> From these counts, the turnover rate is defined as

$$TOR = \frac{G + L}{S + G + L},$$

<sup>44</sup> representing the fraction of pixels that changed between consecutive frames. This pixel-based  
<sup>45</sup> strategy follows earlier microglial motility work ([M. Fuhrmann et al., 2010](#); [Nebeling et al., 2023](#)) while providing a fully automated and batchable implementation with parameter logging  
<sup>46</sup> and diagnostics.

<sup>48</sup> The pipeline exposes options for 3D or 2D registration, contrast-limited adaptive histogram  
<sup>49</sup> equalization, histogram matching across time to mitigate bleaching, and median or Gaussian  
<sup>50</sup> filtering ([Pizer et al., 1987](#); [Virtanen et al., 2020](#); [Walt et al., 2014](#)). Results include segmented  
<sup>51</sup> images, G/L/S/TOR values, brightness and area traces, and spreadsheets for downstream  
<sup>52</sup> statistics. Memory-efficient reading and chunked processing of large TIFFs are supported via  
<sup>53</sup> Zarr ([Miles et al., 2025](#)).

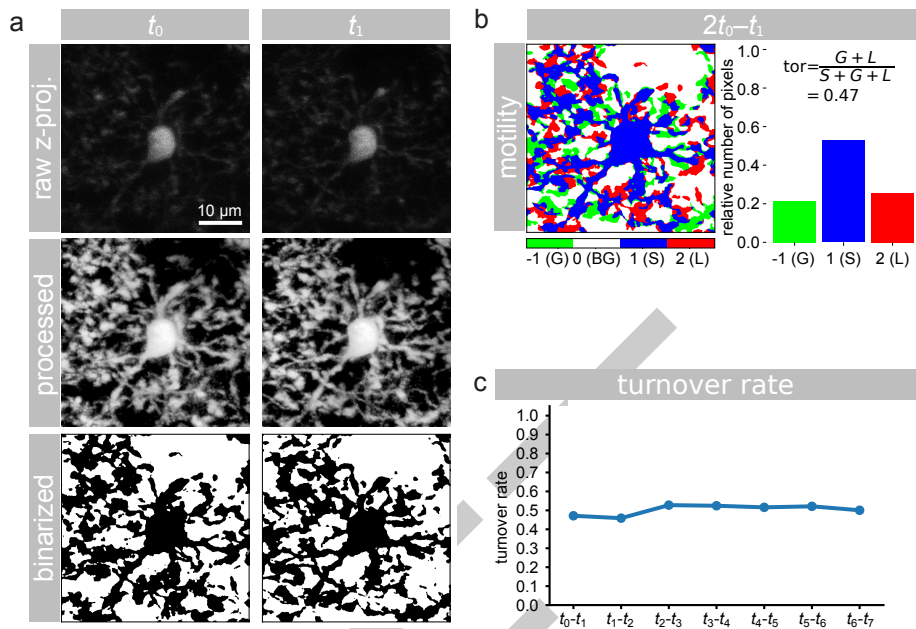


**Figure 1:** Example analysis with MotilA. **a)** z-projected microglial images at two consecutive time points ( $t_0$ ,  $t_1$ ), shown as raw, processed, and binarized data. **b)** pixel-wise classification of gained (G), stable (S), and lost (L) pixels used to compute the turnover rate (TOR). **c)** TOR values across time points from the same dataset, illustrating dynamic remodeling of microglial fine processes.

## 54 Usage

55 MotilA can be called from Python scripts or Jupyter notebooks. Three entry points cover  
 56 common scenarios: `process_stack` for a single stack, `batch_process_stacks` for a project  
 57 folder organized by dataset identifiers with a shared metadata sheet, and `batch_collect` to  
 58 aggregate metrics across datasets. All steps write intermediate outputs and logs to facilitate  
 59 validation and reproducibility. MotilA's GitHub repository provides tutorials and an example  
 60 dataset to shorten onboarding.

## 61 Applications and scope

62 MotilA has been applied to quantify microglial process dynamics in several *in vivo* imaging  
 63 studies and preprints (Crux et al., 2024; F. Fuhrmann et al., 2024; Gockel et al., 2025). Typical  
 64 use cases include baseline surveillance behavior, responses to neuroinflammation or genetic  
 65 perturbations, and deep three-photon imaging where manual analysis is impractical. The  
 66 binarize-and-compare principle can in principle be adapted to other structures such as dendrites  
 67 or axons when segmentation across time is robust.

## 68 Limitations

69 Using 2D projections simplifies processing but sacrifices axial specificity and can merge  
 70 overlapping structures. Segmentation quality determines accuracy and can be affected by  
 71 vessels, low signal-to-noise ratios, or strong intensity drift. The current spectral unmixing is a  
 72 simple subtraction; advanced approaches may be needed for some fluorophores. MotilA targets  
 73 pixel-level process motility rather than object-level tracking or full morphometry.

74    **Example dataset**

75    The repository includes two *in vivo* two-photon stacks from mouse frontal cortex formatted for  
76    use with *MotilA* (Gockel et al., 2025). Each stack contains eight time points at five-minute  
77    intervals, two channels for microglia and neurons, and approximately sixty z-planes at one  
78    micrometer steps in a field of view of about 125 by 125 micrometers. The example reproduces  
79    the full analysis, including projections, segmentation, change maps, brightness traces, and  
80    TOR over time, and serves as a template for cohort-level workflows.

81    **Availability**

82    Source code, documentation, tutorials, and issue tracking are hosted at: <https://github.com/FabrizioMusacchio/motila>. The software runs on Windows, macOS, and Linux with Python 3.9  
83    or newer and standard scientific Python stacks. It is released under GPL-3.0, and contributions  
84    via pull requests or issues are welcome.  
85

86    **Acknowledgements**

87    We thank the Light Microscopy Facility and Animal Research Facility at the DZNE, Bonn, for  
88    essential support. This work was supported by the DZNE and grants to MF from the ERC  
89    (MicroSynCom 865618) and the DFG (SFB1089 C01, B06; SPP2395). MF is a member of  
90    the DFG Excellence Cluster ImmunoSensation2. Additional support came from the iBehave  
91    network and the CANTAR network funded by the Ministry of Culture and Science of North  
92    Rhine-Westphalia, and from the Mildred-Scheel School of Oncology Cologne-Bonn. Animal  
93    procedures followed institutional and national regulations, with efforts to reduce numbers and  
94    refine conditions.

95    **References**

- 96    Brown, D. L. (2017). Bias in image analysis and its solution: Unbiased stereology. *Journal of Toxicologic Pathology*, 30(3), 183–191. <https://doi.org/10.1293/tox.2017-0013>
- 97    Carl Zeiss Microscopy GmbH. (Accessed 2025). ZEISS ZEN Microscopy Software. <https://www.zeiss.com/metrology/en/software/zeiss-zен-core.html>.
- 98    Crux, S., Roggan, M. D., Poll, S., Nebeling, F. C., Schiweck, J., Mittag, M., Musacchio, F.,  
99    Steffen, J., Wolff, K. M., Baral, A., Witke, W., Gurniak, C., Bradke, F., & Fuhrmann,  
100    M. (2024). Deficiency of actin depolymerizing factors ADF/Cfl1 in microglia decreases  
101    motility and impairs memory. *bioRxiv*. <https://doi.org/10.1101/2024.09.27.615114>
- 102    Fuhrmann, F., Nebeling, F. C., Musacchio, F., Mittag, M., Poll, S., Müller, M., Giovannetti, E.  
103    A., Maibach, M., Schaffran, B., Burnside, E., Chan, I. C. W., Lagurin, A. S., Reichenbach,  
104    N., Kaushalya, S., Fried, H., Linden, S., Petzold, G. C., Tavosanis, G., Bradke, F., &  
105    Fuhrmann, M. (2024). Three-photon *in vivo* imaging of neurons and glia in the medial  
106    prefrontal cortex with sub-cellular resolution. *bioRxiv*. <https://doi.org/10.1101/2024.08.28.610026>
- 107    Fuhrmann, M., Bittner, T., Jung, C. K. E., Burgold, S., Page, R. M., Mitteregger, G., Haass,  
108    C., LaFerla, F. M., Kretzschmar, H., & Herms, J. (2010). Microglial Cx3cr1 knockout  
109    prevents neuron loss in a mouse model of alzheimer's disease. *Nature Neuroscience*, 13(4),  
110    411–413. <https://doi.org/10.1038/nn.2511>
- 111    Gockel, N., Nieves-Rivera, N., Druart, M., Jaako, K., Fuhrmann, F., Rožkalne, R., Musacchio,  
112    F., Poll, S., Jansone, B., Fuhrmann, M., & Magueresse, C. L. (2025). Example datasets for  
113    microglial motility analysis using the MotilA pipeline. Zenodo. <https://doi.org/10.5281/zenodo.15061566>
- 114    Miles, A., jakirkham, Hamman, J., Orfanos, D. P., Stansby, D., Bussonnier, M., Moore,  
115    J., Bennett, D., Augspurger, T., Rzepka, N., Cherian, D., Verma, S., Bourbeau, J.,

- 120 Fulton, A., Abernathey, R., Lee, G., Spitz, H., Kristensen, M. R. B., Jones, M., &  
121 Schut, V. (2025). *Zarr-developers/zarr-python: v3.0.6* (Version v3.0.6). Zenodo. <https://doi.org/10.5281/zenodo.3773449>
- 123 Nebeling, F. C., Poll, S., Justus, L. C., Steffen, J., Keppler, K., Mittag, M., & Fuhrmann,  
124 M. (2023). Microglial motility is modulated by neuronal activity and correlates with  
125 dendritic spine plasticity in the hippocampus of awake mice. *eLife*, 12, e83176. <https://doi.org/10.7554/eLife.83176>
- 127 Nimmerjahn, A., Kirchhoff, F., & Helmchen, F. (2005). Resting microglial cells are highly  
128 dynamic surveillants of brain parenchyma in vivo. *Science*, 308(5726), 1314–1318. <https://doi.org/10.1126/science.1110647>
- 130 Pizer, S. M., Amburn, E. P., Austin, J. D., Cromartie, R., Geselowitz, A., Greer, T., Haar  
131 Romeny, B. ter, Zimmerman, J. B., & Zuiderveld, K. (1987). Adaptive histogram equaliza-  
132 tion and its variations. *Computer Vision, Graphics, and Image Processing*, 39(3), 355–368.  
133 [https://doi.org/10.1016/S0734-189X\(87\)80186-X](https://doi.org/10.1016/S0734-189X(87)80186-X)
- 134 Prinz, M., Jung, S., & Priller, J. (2019). Microglia biology: One century of evolving concepts.  
135 *Cell*, 179(2), 292–311. <https://doi.org/10.1016/j.cell.2019.08.053>
- 136 Schindelin, J., Arganda-Carreras, I., Frise, E., Kaynig, V., Longair, M., Pietzsch, T., Preibisch,  
137 S., Rueden, C., Saalfeld, S., Schmid, B., & others. (2012). Fiji: An open-source platform  
138 for biological-image analysis. *Nature Methods*, 9(7), 676–682. <https://doi.org/10.1038/nmeth.2019>
- 140 Tremblay, M.-È., Lowery, R. L., & Majewska, A. K. (2010). Microglial interactions with  
141 synapses are modulated by visual experience. *PLOS Biology*, 8(11), 1–16. <https://doi.org/10.1371/journal.pbio.1000527>
- 143 Virtanen, P., Gommers, R., Oliphant, T. E., Haberland, M., Reddy, T., Cournapeau, D.,  
144 Burovski, E., Peterson, P., Weckesser, W., Bright, J., Walt, S. J. van der, Brett, M.,  
145 Wilson, J., Millman, K. J., Mayorov, N., Nelson, A. R. J., Jones, E., Kern, R., Larson, E., ...  
146 Contributors, S. 1.0. (2020). SciPy 1.0: Fundamental algorithms for scientific computing  
147 in python. *Nature Methods*, 17, 261–272. <https://doi.org/10.1038/s41592-019-0686-2>
- 148 Wall, E., Blaha, L. M., Paul, C. L., Cook, K., & Endert, A. (2018). Four perspectives on  
149 human bias in visual analytics. In G. Ellis (Ed.), *Cognitive biases in visualizations* (pp.  
150 29–42). Springer International Publishing. [https://doi.org/10.1007/978-3-319-95831-6\\_3](https://doi.org/10.1007/978-3-319-95831-6_3)
- 151 Walt, S. van der, Schönberger, J. L., Nunez-Iglesias, J., Boulogne, F., Warner, J. D., Yager,  
152 N., Gouillart, E., Yu, T., & contributors, the scikit-image. (2014). Scikit-image: Image  
153 processing in python. *PeerJ*, 2, e453. <https://doi.org/10.7717/peerj.453>